Supporting Information

Solution-processed tungsten oxide with Ta^{5+} doping enhances the hole selective transport for crystalline silicon solar cells

Dan Liu[a], Penghui Ren[a], Di Zhao[a], Songyu Li[a], Jianqiao Wang[a], Hang Zhou[a], Wei Liu[b], Yuheng Zeng[b], Xuegong Yu[c], Peng Wang[a]*, Can Cui[a]*

[a]Zhejiang Key Laboratory of Quantum State Control and Optical Field Manipulation, Department of Physics, Zhejiang Sci-Tech University, Hangzhou, 310018, China

[b]Ningbo Institute of Materials Technology and Engineering, Chinese Academy of Sciences, Ningbo 315201, China

[c]State Key Laboratory of Silicon and Advanced Semiconductor Materials, School of Materials Science and Engineering, Zhejiang University, Hangzhou 310027, China

E-mail: pengwang@zstu.edu.cn, cancui@zstu.edu.cn

The DFT calculation

All models used for calculation in this work were built using Materials Studio 2020 and visualized using VESTA. First-principles calculations based on density functional theory (DFT) were carried out using the Vienna Ab initio Simulation Package (VASP). The Perdew-Burke-Ernzerhof (PBE) functional was employed to describe the exchange-correlation interaction. The plane-wave cut-off energy of 400 eV, and Γ-centered k-mesh with k-spacing of 0.02 Å^{-3} in the Brillouin zone were used for geometry optimization and self-consistent calculation. The convergence criteria for total energy were set to 10^{-8} eV/atom. The van der Waals interaction was considered using DFT-D3 method. Based on the model, we calculated the free energy, ELF and DOS of the system as W^{5+} or W^{6+} is replaced by Ta^{5+}, respectively. The more negative the free energy of the system, the higher probability the substitution takes place.
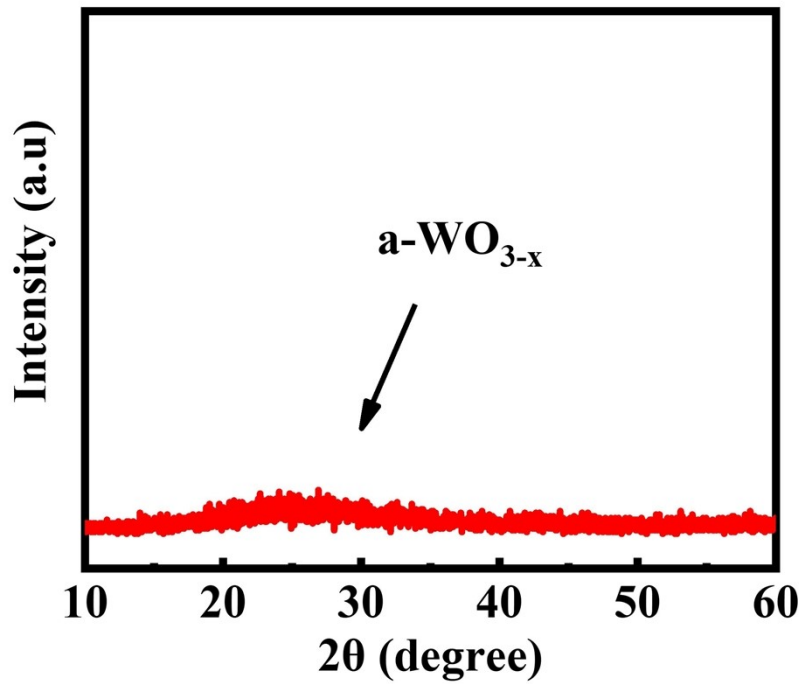
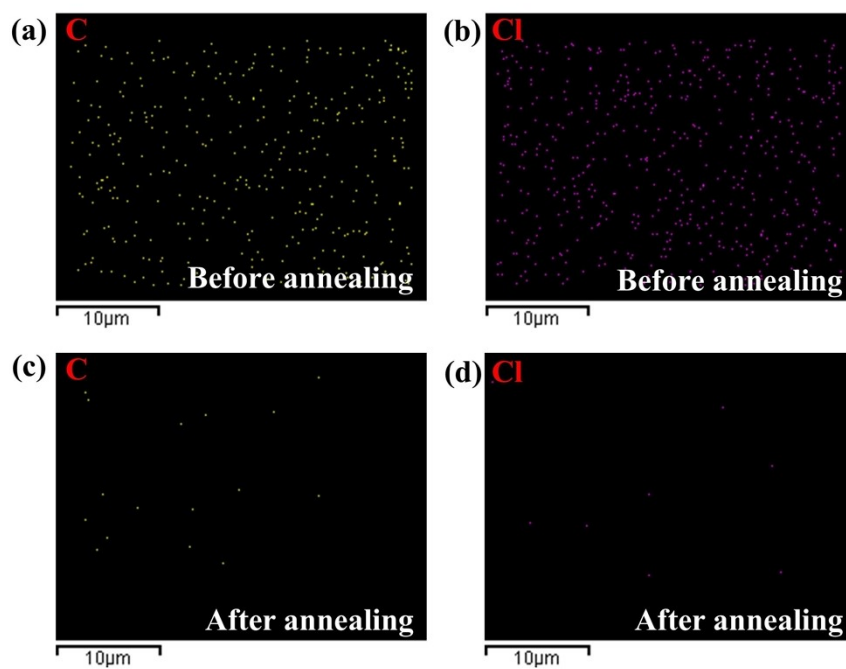**Figure S1.** The XRD pattern of undoped WO_{3-x} film annealed at 100 °C.

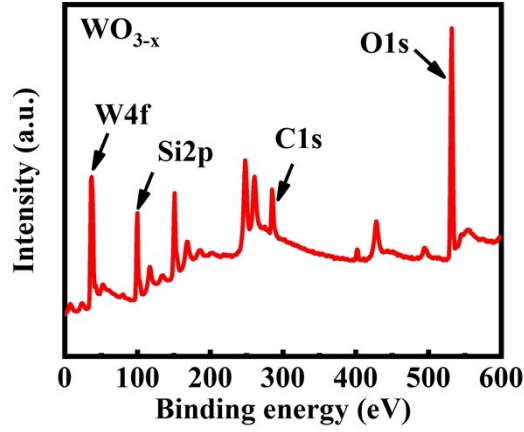**Figure S2.** The EDS mapping images of the undoped WO_{3-x} films (a, b) before and after (c, d) annealing at 100°C.

Figure S3. The XPS spectrum of the undoped WO_{3-x} film after annealing at 100°C.
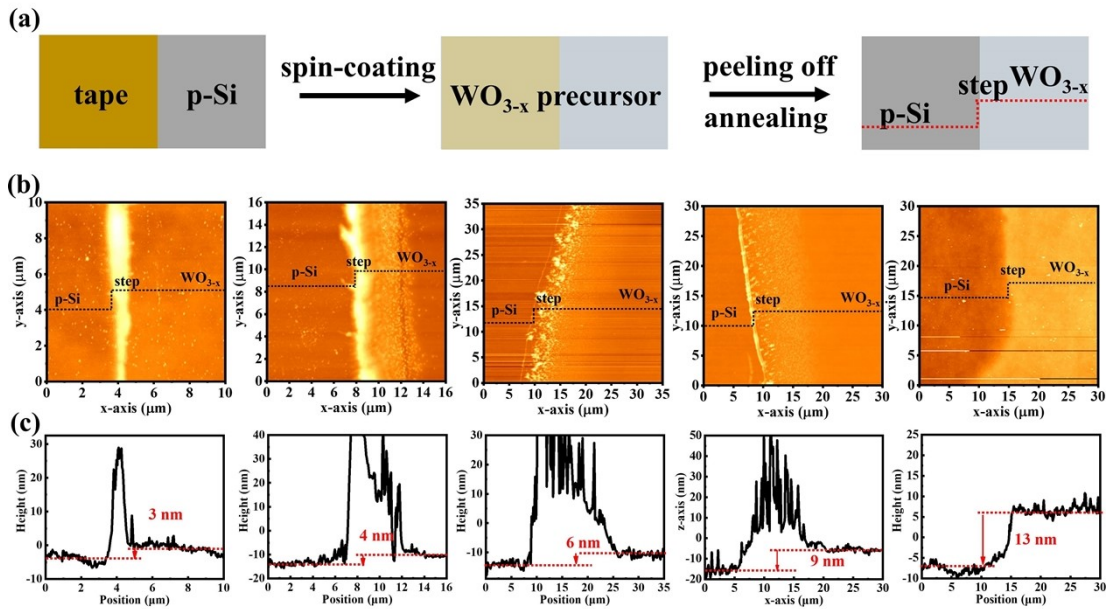

Figure S4. AFM measurements employed to estimate the thickness of undoped WO_{3-x} films. (a) The schematic diagram of AFM measurements. (b) The AFM images of WO_{3-x} films with different thicknesses. (c) Height plots showing the thicknesses of WO_{3-x} films.
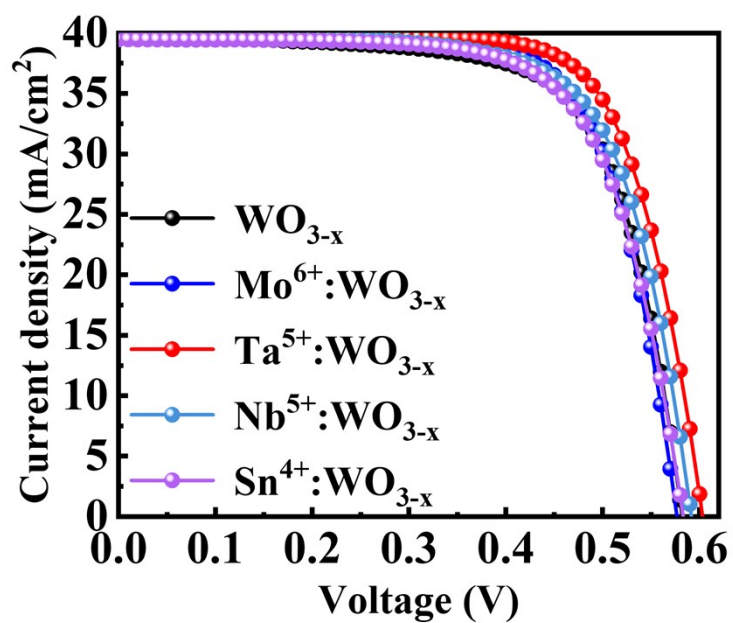
Figure S5. Illuminated *J-V* curves of heterojunction devices with WO_{3-x} films doped with ions of different valence states (Mo^{6+}, Ta^{5+}, Nb^{5+}, Sn^{4+}).
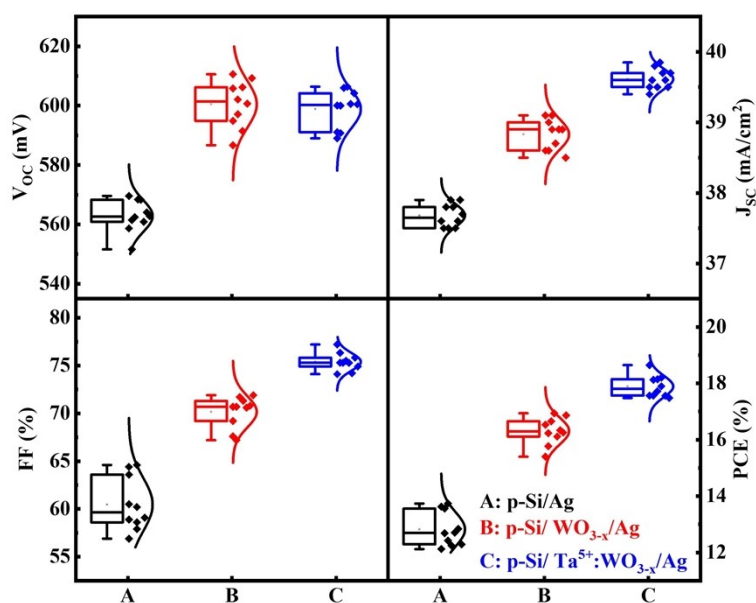

Figure S6. Device performance statistics with the structure of p-Si/Ag, p-Si/WO_{3-x}/Ag and p-Si/Ta^{5+}(1%):WO_{3-x} /Ag.
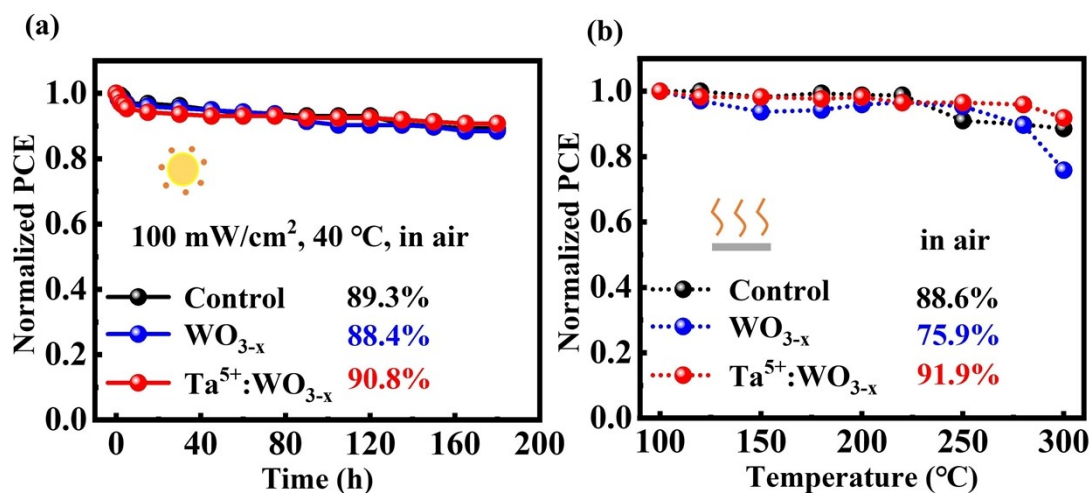
Figure S7. (a) The operational stability of the solar cells with the structure of p-Si/Au/Ag, p-Si/WO$_{3-x}$/Au/Ag and p-Si/Ta^{5+}(1%):WO$_{3-x}$/Au/Ag measured under continuous light illumination (100 mW/cm^2) at the temperature of 40 °C in air. (b) Thermal stability of the devices at different temperatures in air.

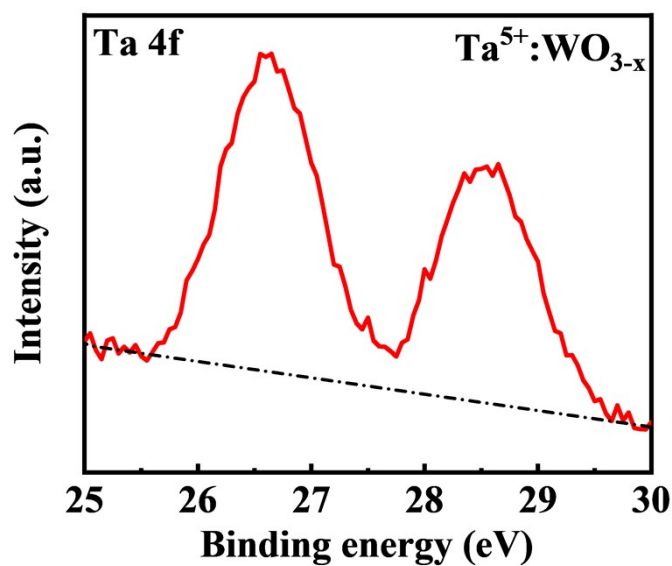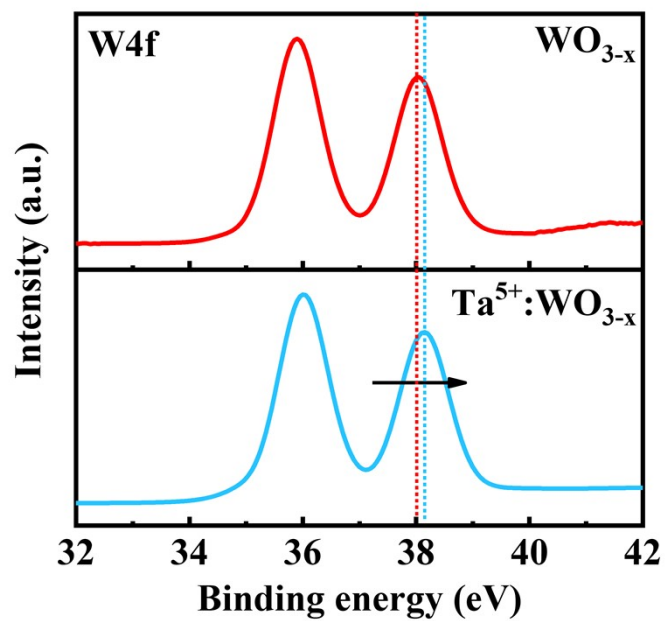**Figure S8**. XPS spectra of Ta 4f orbitals of Ta^{5+}(1%):WO$_{3-x}$ films.

Figure S9. XPS spectra of W 4f orbitals of undoped and 1% Ta^{5+} doped WO_{3-x} films.
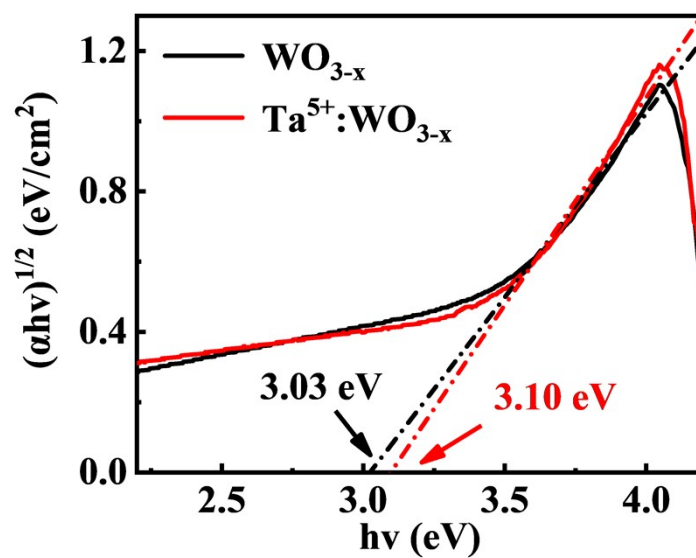

Figure S10. Fitted bandgaps of undoped and 1% Ta^{5+} doped WO_{3-x} films.

Table S1 Output parameters of WO_{3-x}/p-Si heterojunction solar cells with different film thicknesses.

Thickness (nm)	V_{OC} (mV)	J_{SC} (mA/cm^2)	FF (%)	PCE (%)
0	560.9	37.6	58.6	12.4
3	569.9	38.5	63.4	13.9
4	570.9	38.6	63.6	14.0
6	573.6	38.7	68.7	15.3
9	583.5	39.0	70.2	16.0
13	586.4	38.6	68.4	15.5

Table S2 Output parameters of WO_{3-x}/p-Si heterojunction solar cells with different ion doping.

Film	V_{OC} (mV)	J_{SC} (mA/cm^2)	FF (%)	PCE (%)
WO_{3-x}	582.3	39.2	69.6	15.9
Mo^{6+}:WO_{3-x}	576.8	39.8	71.6	16.5
Ta^{5+}:WO_{3-x}	603.1	39.8	73.0	17.5
Nb^{5+}:WO_{3-x}	591.7	39.8	70.2	16.5
Sn^{4+}:WO_{3-x}	583.2	39.3	69.4	15.9

Table S3. Simulation parameters of WO_{3-x}/p-Si heterojunction without and with Ta^{5+} doping.

Parameters	p-Si	WO_{3-x}	$Ta^{5+}:WO_{3-x}$
Layer thickness (cm)	1.5×10^{-2}	1×10^{-6}	1×10^{-6}
Doping concentration (cm^{-3})	$N_a=1\times10^{14}$	$N_d=1\times10^{17}$	$N_d=1\times10^{15}$
Relative dielectric constant	11.9	10	10
Electron affinity (eV)	4.05	4.64	4.69
Band gap (eV)	1.124	3.03	3.10
Optical band gap (eV)	1.124	3.03	3.10
Effective conduction band density (cm^{-3})	2.846×10^{19}	5.0×10^{20}	5.0×10^{20}
Effective valence band density (cm^{-3})	2.685×10^{19}	5.0×10^{20}	5.0×10^{20}
Electron mobility (cm^2/Vs)	1041	10	10
Hole mobility (cm^2/Vs)	412.9	1	1

The *film thickness*, *band gap*, *optical band gap* and *electron affinity* are obtained from the experimental results. The other simulation parameters of Table S3 are cited from the references of H. Mehmood et al., *Renew. Energy*, 2022, **183**, 188-201; R. A. Vijayan et al., *IEEE J. Photovolt.*, 2018, **8**, 473-482.